

# Fluorescence Lifetimes and Quantum Yields of Rhodamine Derivatives: New Insights from Theory and Experiment

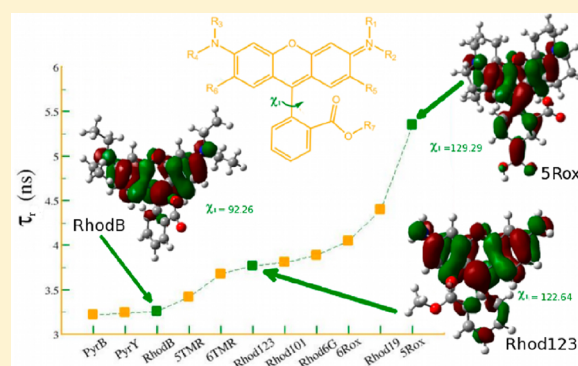
Marika Savarese,<sup>†,‡</sup> Anna Aliberti,<sup>‡</sup> Ilaria De Santo,<sup>‡</sup> Edmondo Battista,<sup>‡</sup> Filippo Causa,<sup>‡</sup> Paolo A. Netti,<sup>‡</sup> and Nadia Rega<sup>\*,†,‡</sup>

<sup>†</sup>Dipartimento di Scienze Chimiche, Università di Napoli 'Federico II', Complesso Universitario di M.S. Angelo, via Cintia, I-80126 Napoli, Italy

<sup>‡</sup>Center for Advanced Biomaterials for Health Care@CRIB, Istituto Italiano di Tecnologia, Largo Barsanti e Matteucci 53, I-80125 Napoli, Italy

## S Supporting Information

**ABSTRACT:** Although lifetimes and quantum yields of widely used fluorophores are often largely characterized, a systematic approach providing a rationale of their photophysical behavior on a quantitative basis is still a challenging goal. Here we combine methods rooted in the time-dependent density functional theory and fluorescence lifetime imaging microscopy to accurately determine and analyze fluorescence signatures (lifetime, quantum yield, and band peaks) of several commonly used rhodamine and pyronin dyes. We show that the radiative lifetime of rhodamines can be correlated to the charge transfer from the phenyl toward the xanthene moiety occurring upon the  $S_0 \leftarrow S_1$  de-excitation, and to the xanthene/phenyl relative orientation assumed in the  $S_1$  minimum structure, which in turn is variable upon the amino and the phenyl substituents. These findings encourage the synergy of experiment and theory as unique tool to design finely tuned fluorescent probes, such those conceived for modern optical sensors.



## 1. INTRODUCTION

Rhodamine dyes are xanthene derivatives presenting photo-physical properties well suited for a wide range of applications. Due to the advance of techniques based on fluorescence signaling and encoding,<sup>1–5</sup> a renewed interest in synthesis strategies and spectroscopic characterization of these systems has been recently shown in the literature.<sup>6–10</sup> As a matter of fact, a high degree of comprehension is required for a full control and design of modern optical sensors, such as fluorescence encoding multiplex systems.<sup>3–5</sup>

On the other hand, the photophysical behavior of rhodamines is not fully understood or established, in spite of the large amount of studies published along the decades.<sup>11–19</sup> For example, the rationale underlying trends of both radiative and nonradiative decays with respect to structural arrangements has not been identified, and several models have been debated to interpret the quantum yield behavior.<sup>12,14,16–23</sup>

Time-dependent density functional theory (TD-DFT)<sup>24–27</sup> provides an important tool to interpret experimental trends in photochemistry. On the other hand, assessment of TD-DFT as predictive of structure/properties relationships on a quantitative basis is still the subject of an intense research effort.<sup>28–31</sup> In this work we combine calculations based on TD-DFT with fluorescence lifetime imaging microscopy (FLIM)<sup>32</sup> data to determine and systematically analyze fluorescence lifetime and quantum yield of several commonly used rhodamine dyes.

Comparison of calculated and experimental lifetimes allowed us to obtain values of the quantum yield that are in very good agreement with data previously reported in literature. We demonstrate that radiative decay rates are modulated by the interactions involving the two main moieties of the rhodamine, namely, the phenyl and the xanthene rings. These interactions sensibly change upon electronic excitation to the fluorescent state and are finely tuned by the solvent and by both the xanthene and phenyl substituents. The correlation between radiative lifetime and relative orientation of the two molecular moieties is evident already when analyzed on the basis of calculated minimum energy structures, once the excited state energy surface is accurately defined at the quantum mechanical level including dispersion energy terms and average solvent effects. The present results point at the combination of TD-DFT and FLIM as a very promising support to perform a rational and well controlled design of fluorescent probes.

In the following section we briefly describe our experimental procedure and computational protocol. We illustrate and discuss the results in section 3 and give our conclusions in section 4.

**Received:** March 5, 2012

**Revised:** May 31, 2012

**Published:** June 6, 2012

## 2. METHODS

**2.1. Experimental Section.** Fluorescence lifetimes of several rhodamine dyes were measured by FLIM. We considered four among the most common rhodamines derivatives, namely commercial Rhodamine B (RhodB), Rhodamine 6G (Rhod6G), 5(6)-Carboxy-tetramethyl-rhodamine (5(6)TMR), and 5(6)-Carboxy-X-rhodamine (5(6)Rox) (Sigma-Aldrich). Measurements were taken at 23 °C of 2  $\mu$ M of dye in acetonitrile solutions freshly prepared. Solution drops were placed on a coverslip and then imaged. Fluorescence lifetime imaging was performed using a Laser Scanning Microscope (TCS SP5, Leica, Wetzlar, Germany), which had an integrated compact Lifetime Upgrade Kit from PicoQuant, Berlin, Germany.

Measurements were carried out in time-tagged time-resolved (TTTR) data acquisition mode (PicoHarp300). Data were analyzed using the built-in SymPhoTime software. A diode laser (PicoQuant LDH Series) provided excitation at 470 nm. RhodB and 5(6)TMR were excited with a laser pulsing rate of 40 MHz, whereas 20 MHz pulsing rate was used for Rhod6G and 5(6)Rox. Emitted fluorescence was monitored over 500–750 nm after passage through 1  $\mu$ m pinhole to get the highest intensity signal, and a scanning rate of 100 Hz was adopted. The images were recorded with 128  $\times$  128 pixels and at least 200 time bins per pixel were collected. A pixel size was 520 nm and the time per pixel 0.006 ms. Dark images were binned twice to increase intensity. The FLIM images were prior binned 2  $\times$  2 and analyzed by a tail-fitting FLIM approach using one or two exponential fit, as needed. The mean of the average lifetimes were determined.

**2.2. Theory and Computational Details.** DFT and TD-DFT methods were exploited to obtain minimum energy structures in both the ground and excited states for two pyronin systems and nine rhodamine derivatives, namely Pyronin B (PyrB), Pyronin Y (PyrY), RhodB, 5TMR, 6TMR, Rhod6G, 5Rox, 6Rox, Rhodamine 123 (Rhod123), Rhodamine 19 (Rhod19), and Rhodamine 101 (Rhod101) (see section 3 for details). Grimme<sup>33</sup> correction energy terms were combined with the B3LYP<sup>34</sup> density functional to account for electronic dispersion interactions (DFT-D). Solvent effects were treated by the conductor-like polarizable continuum model (CPCM),<sup>27,35–37</sup> adopted in the linear response formalism when used with TD-DFT. In this case the solvent reaction field was considered in the regime of equilibrium for geometry optimizations and of nonequilibrium for electronic transition energies calculations. A specific solvent was chosen for each xanthene dye to mimic the experimental conditions of both FLIM measurements (see section 2.1) and lifetime determinations reported in literature. Structure optimizations were performed at the B3LYP-D/6-31+G(d,p)/CPCM and TD-B3LYP-D/6-31+G(d,p)/CPCM levels of theory for the ground and excited states, respectively. Single point energies for ground and excited states were calculated by adopting both B3LYP and long-range corrected<sup>38</sup> CAM-B3LYP<sup>39</sup> functionals. The same levels were exploited to calculate the emission parameters (transition energy, transition electric moment). From these data, radiative lifetime and quantum yields were calculated according to the following protocol.

At a first level of approximation, the emission process can be modeled by a vertical  $S_0 \leftarrow S_1$  transition, i.e., considering as structure of reference the minimum on the excited energy potential.<sup>40,41</sup> According to this model, the spontaneous

emission decay rate  $k_r$  from excited to ground state ( $S_0 \leftarrow S_1$  transition) can be expressed as<sup>42,43</sup>

$$k_r = \frac{4}{3} \frac{\Delta E^3}{c^3} \mu_{10}^2 \quad (1)$$

where  $\Delta E$  is the  $S_0 \leftarrow S_1$  transition energy,  $c$  is the light speed, and  $\mu_{10}^2$  the transition dipole strength in atomic units.

We stress that  $\Delta E$  and  $\mu_{10}$  are evaluated on the minimum structure of the excited state potential energy surface, including averaged solvent effects. Equation 1 can be also compared to eq 20 in ref 44, corresponding to the Strickler–Berg formula for the fluorescence lifetime of molecules.

The radiative lifetime  $\tau_r$  can be therefore obtained as  $\tau_r = 1/k_r$ . Finally, considering the experimental FLIM lifetime  $\tau_{\text{exp}}$  affected by the nonradiative decay rate  $k_{\text{nr}}$  according to  $\tau_{\text{exp}} = 1/(k_r + k_{\text{nr}})$ , we can estimate the quantum yield as the radiative fraction of the total decay rate

$$\Phi = \frac{k_r}{k_r + k_{\text{nr}}} = \frac{\tau_{\text{exp}}}{\tau_r} \quad (2)$$

A fragment analysis of the molecular orbitals was also performed according to the following procedure. We can partition a molecular structure into  $M_{\text{frag}}$  fragments, and we can decompose the electronic density described by a molecular orbital in terms of fragment contributions as

$$C_{\text{frag}} = \sum_j^{n_{\text{frag}}} c_j^2 + \sum_j^{n_{\text{frag}}} \sum_{i < j}^{n_{\text{frag}}} 2c_i c_j S_{ij} \quad (3)$$

where  $i$  and  $j$  run over the  $n_{\text{frag}}$  basis set atomic orbitals centered on nuclei belonging to the fragment,  $c_i$  is the coefficient by which the basis function enters the molecular orbital,  $S_{ij}$  is the basis set overlap matrix element, and

$$\sum_i^{M_{\text{frag}}} C_{\text{frag}_i} = 1 \quad (4)$$

The charge transfer following the  $S_0 \leftarrow S_1$  transition and involving a certain molecular fragment can be therefore expressed as

$$\Delta C_{\text{frag}} = C_{\text{frag}}^{\text{HOMO}} - C_{\text{frag}}^{\text{LUMO}} \quad (5)$$

where the reference structure is the minimum of the  $S_1$  potential energy surface. All the calculations were performed by the Gaussian09<sup>45</sup> suite of programs.

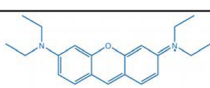
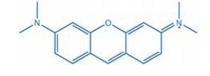

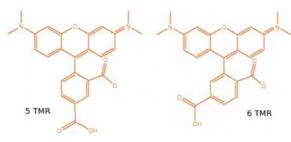
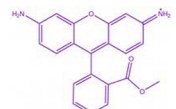
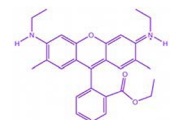

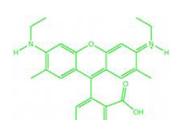
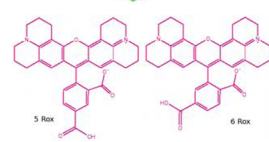
## 3. RESULTS AND DISCUSSION

Structural formula and substituents characterizing the xanthene dyes investigated in the present work are reported in Tables 1 and 2. Abbreviations of commonly used names, adopted hereafter to facilitate the reader, are also reported.

The motif common to all rhodamine dyes is a diaminoxanthene ring with an almost perpendicular carboxyphenyl substituent, this arrangement adopted by symmetry and sterical reasons (Figure 1). The systems chosen in the present work cover a large variety of both amino and phenyl substituents, whereas pyronin systems (diaminoxanthene dyes) were also investigated as reference.

The diaminoxanthene moiety is a cation, and the rhodamine can be in different forms according to the pH and to the phenyl substituent. More specifically, we considered both cations (Rhod6G, Rhod123, Rhod19, along with PyrB and PyrY) and

**Table 1. Short Names and Structural Formula of Xanthene Dyes Considered in the Present Work**

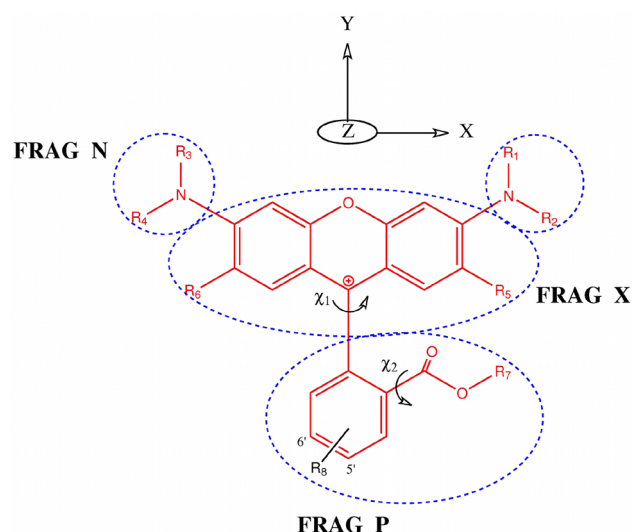
Common name	Abbreviation in this work	Structural formula
Pyronin B	PyrB	
Pyronin Y	PyrY	
Rhodamine B	RhodB	
5(6)-Carboxytetramethyl-rhodamine	5(6)TMR	
Rhodamine 123	Rhod123	
Rhodamine 6G	Rhod6G	
Rhodamine 101	Rhod101	
Rhodamine 19	Rhod19	
5(6)-Carboxy-X-rhodamine	5(6)Rox	

**Table 2. Substituents and Solvents of Xanthene Dyes Considered in the Present Work<sup>a</sup>**

name	amino subst	phenyl subst	solvent
PyrB	R <sub>1</sub> –R <sub>4</sub> = CH <sub>2</sub> CH <sub>3</sub>		water
PyrY	R <sub>1</sub> –R <sub>4</sub> = CH <sub>3</sub>		water
RhodB	R <sub>1</sub> –R <sub>4</sub> = CH <sub>2</sub> CH <sub>3</sub>	R <sub>8</sub> = H	acetonitrile
5(6)TMR	R <sub>1</sub> –R <sub>4</sub> = CH <sub>3</sub>	R <sub>8</sub> = COOH	acetonitrile
Rhod123	R <sub>1</sub> –R <sub>4</sub> = H	R <sub>7</sub> = CH <sub>3</sub> , R <sub>8</sub> = H	ethanol
Rhod6G	R <sub>1</sub> , R <sub>3</sub> = CH <sub>2</sub> CH <sub>3</sub> ; R <sub>2</sub> , R <sub>4</sub> = H	R <sub>7</sub> = CH <sub>2</sub> CH <sub>3</sub> , R <sub>8</sub> = H	acetonitrile
Rhod101	R <sub>1</sub> –R <sub>4</sub> = polycyclic	R <sub>8</sub> = H	ethanol
Rhod19	R <sub>1</sub> , R <sub>3</sub> = CH <sub>2</sub> CH <sub>3</sub> ; R <sub>2</sub> , R <sub>4</sub> = H	R <sub>7</sub> = H, R <sub>8</sub> = H	methanol
5(6)Rox	R <sub>1</sub> –R <sub>4</sub> = polycyclic	R <sub>8</sub> = COOH	acetonitrile

<sup>a</sup>Xanthene substituents R<sub>5</sub> and R<sub>6</sub> are CH<sub>3</sub> in Rhod19, and H elsewhere. Please see Figure 1 for labels.

neutral molecules (RhodB, 5TMR, 6TMR, Rhod101, 5Rox, 6Rox). The theoretical treatment of environmental effects was performed to be consistent with experimental conditions of

**Figure 1.** General structural formula, labeling, and fragment decomposition of the xanthene dyes studied in the present work.

lifetime measurements, and solvents used for each system are listed in Table 2 as well. FLIM measurements provided in the present work were performed in acetonitrile to represent a nonprotic solvent with average polarity (relative permittivity  $\epsilon = 37$ ). Other solvents were chosen on the basis of data available in literature.

**3.1. Structural Analysis in the  $S_0$  and  $S_1$  States.** In Table 3 we report  $\chi_1$  and  $\chi_2$  dihedral angles (Figure 1) of the

**Table 3.  $\chi_1$  and  $\chi_2$  Dihedral Angles (degrees) of Rhodamine Dyes Optimized in the Ground  $S_0$  and First Excited Singlet  $S_1$  State at the B3LYP-D/6-31+G(d,p)/CPCM and TD-B3LYP-D/6-31+G(d,p)/CPCM Levels of Theory**

	$ \chi_1 $		$ \chi_2 $	
	$S_0$	$S_1$	$S_0$	$S_1$
RhodB	94.8	92.3	0.0	0.0
5TMR	94.6	92.4	0.0	4.7
6TMR	94.9	94.4	0.1	0.5
Rhod123	94.4	122.6	2.6	22.9
Rhod6G	115.2	127.3	25.5	37.9
Rhod101	117.6	123.6	33.8	39.2
Rhod19	111.0	126.9	16.5	12.7
5Rox	116.1	129.3	33.4	34.1
6Rox	117.5	124.9	40.1	42.0

rhodamines optimized in both the ground  $S_0$  and the excited  $S_1$  states at the B3LYP-D/6-31+G(d,p) and TD-B3LYP-D/6-31+G(d,p) levels, respectively.

Dihedral angle  $\chi_1$  represents the relative orientation of the phenyl and the xanthene rings, whereas angle  $\chi_2$  describes the rotation of the carboxy group with respect to the phenyl ring. Therefore, variation from the  $\chi_1 = 90^\circ$  and  $\chi_2 = 0^\circ$  arrangement accounts for the overall distortion of the two main moieties in rhodamine from the  $C_s$  symmetry. X-ray structures exhibit a symmetric arrangement in Rhod123 and a deviation of about  $33^\circ$  from the full symmetry in Rhod6G.<sup>46</sup> This distortion, however, was attributed to crystal packing effects and previous calculations suggested a symmetrical Rhod6G structure.<sup>47</sup>

Concerning our results in the ground state, from inspection of Table 3, we note that RhodB, 5TMR, 6TMR, and Rhod123



adopt an almost symmetrical arrangement, whereas a variable and consistent distortion is observed for Rhod6G, Rhod101, 5Rox, and 6Rox. The cationic Rhod19 (carboxylic group as phenyl substituent) also shows a less important, but significant, distortion ( $|\chi_1| \cong 110^\circ$ ). These results reproduce the different behavior shown by crystallographic structures of Rhod123 and Rhod6G and demonstrate how the minimum energy arrangement may be driven by several forces. In fact,  $\chi_1/\chi_2$  distortion can result from a subtle balance of Coulombic and nonclassical interactions involving the two rings and the solvent.  $C_s$  symmetry is favored by Coulombic attraction and steric repulsion between the polar carboxy group and the positively charged xanthene. Asymmetry, on the other hand, can lead to stabilizing dispersion interactions between the carboxy substituent and the xanthene. Moreover, distortion may enhance the carboxylic oxygen exposure to the polar solvent, leading to more stabilizing solute–solvent interactions.

After the electronic excitation to the  $S_1$  state, RhodB, 5TMR, and 6TMR maintain the ground state  $C_s$  symmetry. The methyl ester substituted Rhod123, on the other hand, switches from the almost symmetrical  $S_0$  structure to a largely distorted arrangement ( $|\chi_1| = 123^\circ$ ) in  $S_1$ . The remaining rhodamines exhibit an enhancement of about  $10^\circ$  for both the  $\chi_1$  and  $\chi_2$  angles upon the excitation. Recently, a  $\chi_1$  distortion upon electronic excitation has been calculated for the tetramethyl isothiocyanate rhodamine in water,<sup>48</sup> whereas a different  $\chi_1$  adopted in the ground and excited state has been hypothesized to explain the Stokes shift of Rhod19 experimentally recorded in the gas phase.<sup>9</sup>

**3.2. Absorption and Emission Energy.** A detailed discussion about the absorption and emission spectra of the xanthene dyes is out of the main purpose of the present work; nevertheless some important comments are in order after inspection of Table 4, where we report a summary of the

**Table 4. Absorption and Emission Energies (eV) of Pyronin and Rhodamine Dyes Calculated at the TD-B3LYP-D/6-31+G(d,p)/CPCM Level of Theory along with Experimental Counterparts<sup>a</sup>**

	absorption energy		emission energy	
	TD-DFT	exp	TD-DFT	exp
PyrB	2.61	2.27 <sup>a</sup>	2.34	2.14 <sup>b</sup>
PyrY	2.64	2.24 <sup>a</sup>	2.35	2.17 <sup>b</sup>
RhodB	2.66	2.29 <sup>c</sup>	2.41	2.18 <sup>c</sup>
5TMR	2.66	2.28 <sup>d</sup>	2.40	2.18 <sup>d</sup>
6TMR	2.66	2.28 <sup>d</sup>	2.40	2.18 <sup>d</sup>
Rhod123	2.88	2.43 <sup>e</sup>	2.51	2.33 <sup>c</sup>
Rhod6G	2.69	2.59 <sup>f</sup>	2.36	2.23 <sup>c</sup>
Rhod101	2.52	2.20 <sup>c</sup>	2.26	2.11 <sup>c</sup>
Rhod19	2.70	2.40 <sup>c</sup>	2.32	2.28 <sup>c</sup>
5Rox	2.46	2.18 <sup>d</sup>	2.10	2.08 <sup>d</sup>
6Rox	2.49	2.18 <sup>d</sup>	2.21	2.08 <sup>d</sup>

<sup>a</sup>Reference 55. <sup>b</sup>Reference 56. <sup>c</sup>Reference 57. <sup>d</sup>Reference 58. <sup>e</sup>Reference 59. <sup>f</sup>Reference 60.

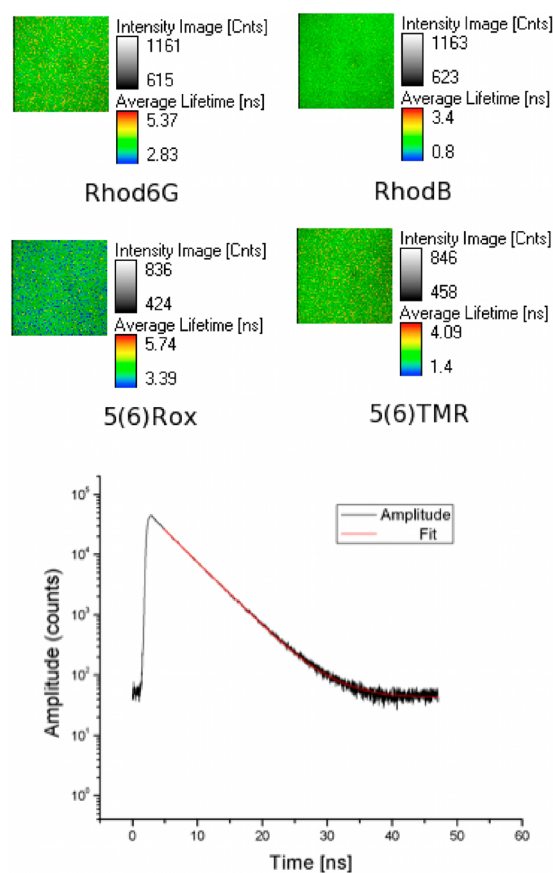
absorption and emission frequencies calculated at the TD-DFT level for all the pyronin and rhodamine dyes, compared to the corresponding experimental data.

According to a general trend of TD-DFT methods,<sup>49,50</sup> previously reported calculations overestimate the rhodamine absorption band peak of about 0.4 eV.<sup>48,51,52</sup> Computational

results can ameliorate when solvent or dynamical effects are taken into account.<sup>48</sup>

Our results show the same trend, although the agreement with the experiment improves when the emission energy is considered. In this case we obtain an average error of 0.15 eV with a standard deviation of 0.007 eV. We can reasonably conclude that our TD-DFT calculations provide a comparable accuracy in all cases considered. This consistency is an important prerequisite to pursue further our comparative analysis of rhodamine dyes, because the emission energy, along with the corresponding dipole strength, determine the radiative decay rate  $k_r$  according to eq 1.

**3.3. Lifetimes and Quantum Yields.** Typical lifetime images recorded in the present work are shown in Figure 2.



**Figure 2.** Upper panel: lifetime images of rhodamines recorded in the present work (acetonitrile solutions at temperature  $T = 23^\circ\text{C}$ ). Images are  $128 \times 128$  pixel and binned  $2 \times 2$ . Pixel size 520 nm. Lower panel: typical fluorescence intensity decay and tail-fitting representative curve obtained for rhodamines.

They refer to RhodB, Rhod6G, and a mixture of isomers in the case of 5(6)TMR and 5(6)Rox, respectively. The determined average lifetimes are listed in Table 5. Regarding the remaining set of pyronines and rhodamines, we report lifetime data provided from literature.

According to the theory discussed in section 2.2, radiative lifetime  $\tau_r$  and quantum yields  $\Phi$  can be calculated by eqs 1 and 2 (see section 2.2). Results are listed in Table 5. Calculated quantum yields  $\Phi$  are also compared to experimental counterparts  $\Phi_{\text{exp}}$  reported from literature, when consistent data in terms of experimental conditions and reference standard are available.

**Table 5. Experimental and Calculated Lifetimes (ns) and Quantum Yields of Pyronin and Rhodamine Dyes**

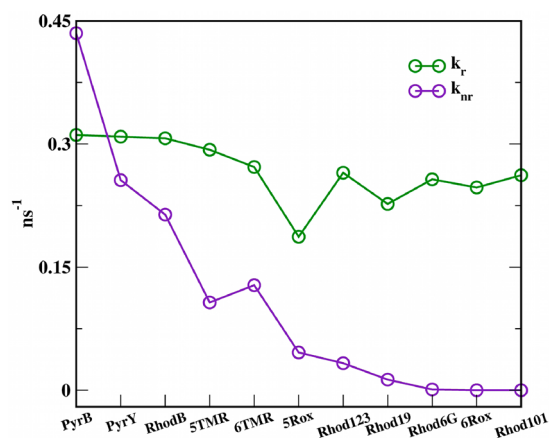
	$\tau_{\text{exp}}$	$\tau_r$	$\Phi$	$\Phi_{\text{exp}}$
PyrB	1.34 <sup>a</sup>	3.22	0.42	0.40, <sup>a</sup> 0.36 <sup>b</sup>
PyrY	1.77 <sup>a</sup>	3.24	0.55	0.35, <sup>a</sup> 0.47 <sup>b</sup>
RhodB	1.92 <sup>c</sup>	3.26	0.59	0.53 <sup>d</sup>
5TMR	2.50 <sup>c</sup>	3.42	0.73	
6TMR	2.50 <sup>c</sup>	3.68	0.68	
Rhod123	3.60 <sup>e</sup>	3.77	0.89	0.90 <sup>f</sup>
Rhod6G	3.87 <sup>c</sup>	3.89	0.99	0.95 <sup>f</sup>
Rhod101	4.10 <sup>g</sup>	3.81	1.08	0.96, <sup>f</sup> 0.98 <sup>h</sup>
Rhod19	4.16 <sup>i</sup>	4.40	0.94	0.95 <sup>f</sup>
5Rox	4.30 <sup>c</sup>	5.35	0.80	
6Rox	4.30 <sup>c</sup>	4.05	1.06	

<sup>a</sup>Reference 55. <sup>b</sup>Reference 61. <sup>c</sup>This work. <sup>d</sup>Reference 14. <sup>e</sup>Reference 62. <sup>f</sup>Reference 57. <sup>g</sup>Reference 63. <sup>h</sup>Reference 6. <sup>i</sup>Reference 64.

We observe that calculated  $\Phi$  are slightly larger than the corresponding  $\Phi_{\text{exp}}$  values: the overestimation of the TD-DFT emission energy leads to an enhancement of the radiative decay rate and, as a consequence, of the calculated quantum yield.

Nevertheless,  $\Phi$  and  $\Phi_{\text{exp}}$  values are in agreement within an average and maximum error of 0.05 and 0.1, respectively. The experimental trend of the whole set is nicely reproduced, from the low values of pyronines to the value of  $\approx 1.0$  for Rhod101, which is usually considered as a reference of the full quantum yield. This result is a solid argument in favor of the accuracy of our combined experimental/theoretical approach.

In Figure 3 we report calculated radiative and non radiative decay rates ( $k_r$  and  $k_{\text{nr}}$ ) for the xanthene dyes ordered by an increasing value of  $\Phi$ .

**Figure 3.** Calculated nonradiative and radiative decay rates ( $\text{ns}^{-1}$ ) for pyronin and rhodamine dyes.

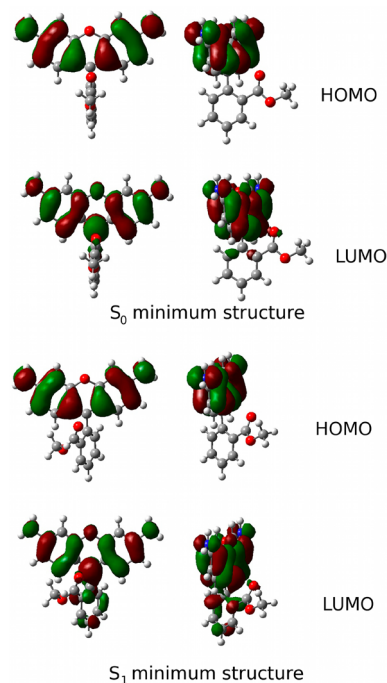
We note that both the  $k_r$  and  $k_{\text{nr}}$  rates generally decrease with the quantum yield, although the  $k_{\text{nr}}$  with a larger derivative. Xanthene dyes with a low quantum yield ( $\Phi < 0.75$ ) correspond to  $k_r$  and  $k_{\text{nr}}$  of the same order of magnitude ( $k_{\text{nr}} > 0.1 \text{ ns}^{-1}$ ).  $k_r$  has been often approximated as a constant with respect to both the rhodamine substituents and the experimental conditions.<sup>11,53</sup> In contrast,  $k_r$  values calculated here cover the not negligible range of  $0.124 \text{ ns}^{-1}$ .

**3.4. Radiative Decay Process.** According to eq 1, the  $S_0 \leftarrow S_1$  radiative decay process depends upon the transition energy  $\Delta E$  and the transition dipole strength  $|\mu_{10}|^2$ . This latter

quantity is increased by the overlap of the ground and the excited electronic density (transition electronic density) along the  $x$  axis of Figure 1, namely along the direction of the  $-\text{N}=\text{C}-\text{C}=\text{C}-\text{O}-\text{C}=\text{C}-\text{C}-\text{N}-$  moiety.<sup>54</sup> On the contrary, transition electronic density involving the phenyl ring ( $yz$  plane) gives a zero contribution to the dipole integral.

At first approximation we can analyze the  $S_0 \leftarrow S_1$  transition electronic energy in terms of the difference between HOMO and LUMO.

Diaminoxanthene systems are characterized by a  $\pi$  HOMO with a nonbonding character located on the xanthene ring and, to some extent, on the amino substituents. The  $\pi^*$  LUMO, on the other hand, is mainly located on the xanthene ring and can be partially located on the phenyl ring, depending on the rhodamine structure. As an example, we report in Figures 4 the

**Figure 4.** HOMO and LUMO countours calculated at the TD-DFT level for Rhod123. Upper panel:  $S_0$  minimum energy structure. Lower panel:  $S_1$  minimum energy structure.

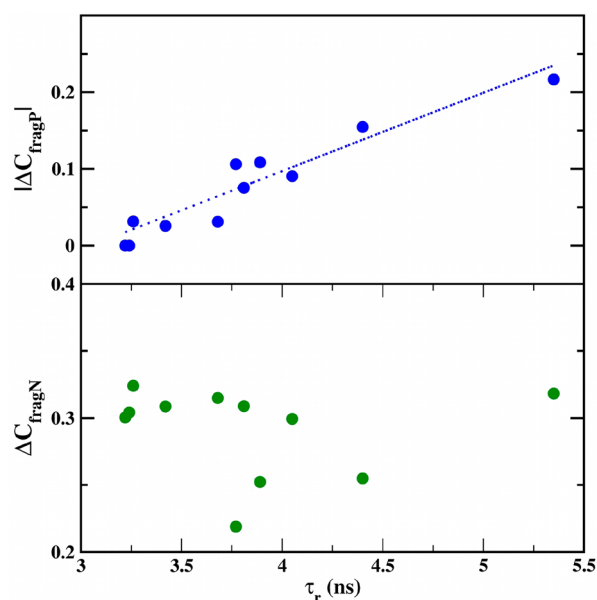
contours of HOMO and LUMO for Rhod123 in the ground and the excited state structure, respectively. We recall that Rhod123 is characterized by a torsion of the phenyl ring with respect the xanthene plane following the  $S_0 \rightarrow S_1$  excitation (Table 3). At variance with the ground state configuration, we note that the excited asymmetrical structure shows a partial location of the LUMO density on the phenyl ring.

On the basis of the considerations above regarding the symmetry of the transition dipole moment, we can expect that a charge transfer involving the phenyl ring upon the  $S_0 \leftarrow S_1$  de-excitation may result in a smaller value of the transition dipole strength  $|\mu_{10}|^2$ , and, as a consequence, a larger fluorescence lifetime  $\tau_r$ .

To verify this hypothesis, we performed the fragment orbital analysis of eqs 3–5 for our set of molecules in the  $S_1$  optimized structures. More precisely we partitioned the rhodamine derivative into three fragments according to the scheme in Figure 1, collecting the xanthene chromophore (FragX), the amino substituents (FragN), and the phenylic group (FragP),

respectively. We then calculated the difference between the HOMO and LUMO contributions from the xanthene ( $\Delta C_{\text{fragX}}$ ), the amino ( $\Delta C_{\text{fragN}}$ ), and the phenyl ( $\Delta C_{\text{fragP}}$ ) fragments, assuming these quantities to be representative of the electronic density rearrangement upon the radiative deactivation process.

The electronic structure of the fragments was analyzed adopting both the B3LYP and the long-range corrected CAM-B3LYP functionals, which gave very similar results. Details are reported as Supporting Information. In Figure 5 we report the



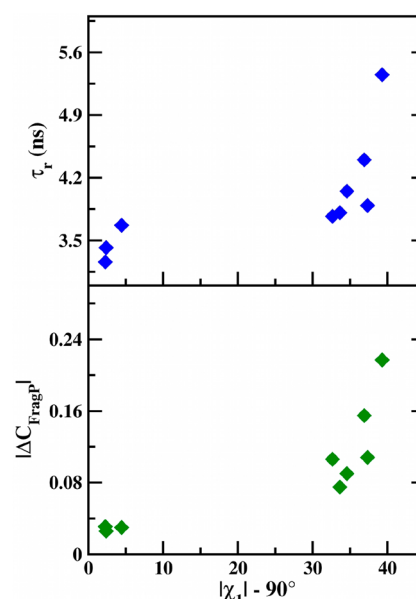
**Figure 5.** Charge transfer from amino and phenyl fragments ( $\Delta C_{\text{fragN}}$  and  $|\Delta C_{\text{fragP}}|$ ) upon the  $S_0 \leftarrow S_1$  de-excitation of rhodamines reported with respect to the corresponding calculated radiative lifetime (ns).

charge transfer involving the phenyl and the amino fragments ( $|\Delta C_{\text{fragP}}|$  and  $\Delta C_{\text{fragN}}$ ) with respect to the radiative lifetime  $\tau_r$  calculated at the B3LYP/6-31+G(d,p) level of theory. We observe a remarkable linear relationship between the radiative property and the charge transfer amount involving the phenyl fragment, whereas no dependence is noticed for the electronic density rearrangement on the amino groups.

As we already observed from inspection of the Rhod123 orbitals, the phenyl involvement can be related to the distortion of the rhodamine structure from the symmetrical arrangement ( $\chi_1 = 90^\circ$ ). In Figure 6 we report both the phenyl charge transfer  $|\Delta C_{\text{fragP}}|$  and the radiative lifetime with respect to the  $\chi_1$  dihedral angle. We note that the increasing of the xanthene–phenyl torsion results in a larger amount of the phenyl  $|\Delta C_{\text{fragP}}|$  and a longer lifetime, with a maximum value of 5.35 ns for the 5Rox ( $|\chi_1| \cong 130^\circ$ ), characterized by a 0.22 electron transfer upon the de-excitation. On the other hand, the  $S_1$  excited state of symmetrical structures ( $\chi_1 \cong 90^\circ$  for RhodB, 5TMR, and 6TMR) is characterized by a shorter fluorescence lifetime ( $\tau_r \cong 3.5$  ns). This result suggests an important structure/property relationship: rhodamine dyes characterized by a xanthene–phenyl distortion in the  $S_1$  minimum structure have larger values of the radiative lifetimes.

#### 4. CONCLUSION

We were able to determine and systematically analyze fluorescence lifetime and quantum yield of several commonly



**Figure 6.** Calculated radiative lifetime (ns) and charge transfer from phenyl fragment upon de-excitation ( $|\Delta C_{\text{fragP}}|$ ) reported with respect to the distortion of the  $\chi_1$  dihedral angle (degrees) of rhodamines.

used rhodamine dyes by combining TD-DFT calculations and FLIM data.

We demonstrate that the photophysical trends in rhodamines are tuned by the interplay of different interactions involving the two main moieties of the molecule, namely the phenyl and the xanthene rings. FLIM data and quantum mechanical calculations of minimum energy structures in the fluorescent excited state can be combined to forecast quantum yield values in good agreement with experimental counterparts. Moreover, the radiative lifetime depends on the amount of charge transfer occurring from the xanthene toward the phenyl group upon the  $S_0 \rightarrow S_1$  excitation. This transfer, on turn, can be related to the xanthene/phenyl relative orientation assumed in the  $S_1$  minimum structure. This orientation is variable upon amino and phenyl substituents, is modulated by the solvent, and, in general, is increased when going from the ground  $S_0$  to the excited  $S_1$  state.

By combining experiment and theory, we provide a procedure to better understand the complex photophysical behavior of fluorescent probes.

#### ■ ASSOCIATED CONTENT

##### Supporting Information

Rhodamine fragment analysis at B3LYP and CAM-B3LYP levels of theory, respectively, charge transfer plots, and complete ref 45. This information is available free of charge via the Internet at <http://pubs.acs.org>

#### ■ AUTHOR INFORMATION

##### Corresponding Author

\*E-mail: [nadia.rega@unina.it](mailto:nadia.rega@unina.it).

##### Notes

The authors declare no competing financial interest.



## ■ ACKNOWLEDGMENTS

N.R. thanks Dr. P. Cimino (University of Salerno) for helpful discussions. She also thanks Gaussian Inc. and MIUR (PRIN2008, protocol 2008J9RNB3\_002) for financial support.

## ■ REFERENCES

- (1) de Silva, A. P.; Gunaratne, H. Q. N.; Gunnlaugsson, T.; Huxley, A. J. M.; McCoy, C. P.; Rademacher, J. T.; Rice, T. E. *Chem. Rev.* **1997**, *97*, 1515–1566.
- (2) Dsouza, R. N.; Pischel, U.; Nau, W. M. *Chem. Rev.* **2011**, *111*, 7941–7980.
- (3) Birtwell, S.; Morgan, H. *Integr. Biol.* **2009**, *1*, 345–362.
- (4) Berezin, M.; Achilefu, S. *Chem. Rev.* **2010**, *110*, 2641–2684.
- (5) Borisov, S.; Wolfbeis, O. *Chem. Rev.* **2008**, *108*, 423–461.
- (6) Beija, M.; Afonso, C.; Martinho, J. *Chem. Soc. Rev.* **2009**, *38*, 2410–2433.
- (7) Koide, Y.; Urano, Y.; Hanaoka, K.; Terai, T.; Nagano, T. *ACS Chem. Biol.* **2011**, *6*, 600–608.
- (8) Larson, D. R.; Ow, H.; Vishwasrao, H. D.; Heikal, A. A.; Wiesner, U.; Webb, W. W. *Chem. Mater.* **2008**, *20*, 2677–2684.
- (9) Chinglin, K.; Balabin, R. M.; Frankevich, V.; Chen, H.; Barylyuk, K.; Nieckarz, R.; Fedorov, A.; Zenobi, R. *Phys. Chem. Chem. Phys.* **2010**, *12*, 14121–14127.
- (10) Chinglin, K.; Balabin, R. M.; Barylyuk, K.; Chen, H.; Frankevich, V.; Zenobi, R. *Phys. Chem. Chem. Phys.* **2010**, *12*, 11710–11714.
- (11) Arbeloa, F. L.; Rohatgi-Mukherjee, K. K. *Chem. Phys. Lett.* **1986**, *129*, 607–614.
- (12) Arbeloa, F. L.; Aguirresacona, I. U. *Chem. Phys.* **1989**, *130*, 371–378.
- (13) Penzkofer, A.; Falkenstein, M. *Opt. Quant. Electron.* **1978**, *10*, 399–423.
- (14) Snare, M.; Treloar, F.; Ghiggino, K.; Thistlethwaite, P. J. *Photochem.* **1982**, *18*, 335–346.
- (15) Karstens, T.; Kobs, K. J. *Phys. Chem.* **1980**, *84*, 1871–1872.
- (16) Drexhage, K. H. *Top. Appl. Phys.* **1973**, *1*, 155–200.
- (17) Drexhage, K. H. *J. Res. Natl. Bur. Stand.* **1976**, *80*, 421–428.
- (18) Vogel, M. W.; Rettig, W.; Sens, R.; Drexhage, K. H. *Chem. Phys. Lett.* **1988**, *147*, 452–460.
- (19) Grabowski, Z.; Rotkiewicz, K.; Siemiarz, A.; Cowley, D. J.; Baumann, W. *Nouv. J. Chim.* **1979**, *3*, 443–454.
- (20) Zachariasse, K. A.; von der Haar, T.; Hebecker, A.; Leinhos, U.; KUhnle, W. *Pure Appl. Chem.* **1993**, *65*, 1745–1750.
- (21) von der Haar, T.; Hebecker, A.; Il'ichev, Y.; Jiang, Y. B.; Ktihnle, W.; Zachariasse, K. A. *Recl. Trav. Chim. Pays-Bas* **1995**, *114*, 430–442.
- (22) Pedone, A.; Prampolini, G.; Monti, S.; Barone, V. *Chem. Mater.* **2011**, *23*, 5016–5023.
- (23) Barone, V.; Bloino, J.; Monti, S.; Pedone, A.; Prampolini, G. *Phys. Chem. Chem. Phys.* **2011**, *13*, 2160–2166.
- (24) Casida, M. E.; Jamorski, C.; Casida, K. C.; Salahub, D. R. *J. Chem. Phys.* **1998**, *108*, 4433–4439.
- (25) Stratmann, R. E.; Scuseria, G. E.; Frisch, M. J. *J. Chem. Phys.* **1998**, *109*, 8218–8224.
- (26) Furche, F.; Ahlrichs, R. *J. Chem. Phys.* **2002**, *117*, 7433–7447.
- (27) Scalmani, G.; Frisch, M. J.; Mennucci, B.; Tomasi, J.; Cammi, R.; Barone, V. *J. Chem. Phys.* **2006**, *124*, 094107 1–15.
- (28) Dreuw, A.; Head-Gordon, M. *Chem. Rev.* **2005**, *105*, 4009–4037.
- (29) Improta, R. *Phys. Chem. Chem. Phys.* **2008**, *10*, 2656–2664.
- (30) Jacquemin, D.; Wathelet, V.; Perpète, E. A.; Adamo, C. *J. Chem. Theor. Comput.* **2009**, *5*, 2420–2435.
- (31) Jacquemin, D.; Mennucci, B.; Adamo, C. *Phys. Chem. Chem. Phys.* **2011**, *13*, 16987–16998.
- (32) Chang, C. W.; Sud, D.; Mycek, M. A. *Meth. Cell. Biol.* **2007**, *81*, 495–524.
- (33) Schwabe, T.; Grimme, S. *Phys. Chem. Chem. Phys.* **2007**, *9*, 3397–3406.
- (34) Becke, A. D. *J. Chem. Phys.* **1993**, *98*, 5648–5652.
- (35) Cossi, M.; Rega, N.; Scalmani, G.; Barone, V. *J. Comput. Chem.* **2003**, *24*, 669–681.
- (36) Cossi, M.; Barone, V. *J. Chem. Phys.* **2000**, *112*, 2427–2435.
- (37) Cossi, M.; Barone, V. *J. Chem. Phys.* **2001**, *115*, 4708–4717.
- (38) Tawada, Y.; Tsuneda, T.; Yanagisawa, S.; Yanai, T.; Hirao, K. *J. Chem. Phys.* **2004**, *120*, 8425–8433.
- (39) Yanai, T.; Tew, D. P.; Handy, N. C. *Chem. Phys. Lett.* **2004**, *393*, 51–57.
- (40) Prieto, J. B.; Arbeloa, F. L.; Martinez, V. M.; Lopez, T. A.; Arbeloa, I. L. *Phys. Chem. Chem. Phys.* **2004**, *6*, 4247–4253.
- (41) Turro, N. J.; Scaiano, J. C.; Ramamurthy, V. *Principles of molecular photochemistry*; University Science Books: Mill Valley, CA, 2009.
- (42) Lounis, B.; Orrit, M. *Rep. Prog. Phys.* **2005**, *68*, 1129–1179.
- (43) Nienhuis, G.; Alkemade, C. T. J. *Physica B+C* **1976**, *81*, 181–188.
- (44) Strickler, S. J.; Berg, R. A. *J. Chem. Phys.* **1962**, *37*, 814–822.
- (45) Frisch, M. J.; Trucks, G. W.; Schlegel, H. B.; Scuseria, G. E.; Robb, M. A.; Cheeseman, J. R.; Scalmani, G.; Barone, V.; Mennucci, B.; Petersson, G. A.; et al. *Gaussian 09*, Revision A.2; Gaussian Inc.: Wallingford, CT, 2009.
- (46) Adhikesavalu, D.; Mastropaolo, D.; Camerman, A.; Camerman, N. *Acta Crystallogr. Sect. C* **2001**, *57*, 657–659.
- (47) Watanabe, H.; Hayazawa, N.; Inouye, Y.; Kawata, S. *J. Phys. Chem. B* **2005**, *109*, 5012–5020.
- (48) Pedone, A.; Bloino, J.; Monti, S.; Prampolini, G.; Barone, V. *Phys. Chem. Chem. Phys.* **2010**, *12*, 1000–1006.
- (49) Jacquemin, D.; Perpète, E.; Vydrov, O.; Scuseria, G.; Adamo, C. *J. Chem. Phys.* **2007**, *127*, 094102 1–6.
- (50) Jacquemin, D.; Perpète, E.; Scalmani, G.; Frisch, M.; Kobayashi, R.; Adamo, C. *J. Chem. Phys.* **2007**, *126*, 1441051–12.
- (51) Guthmuller, J.; Champagne, B. *J. Phys. Chem. A* **2008**, *112*, 3215–3223.
- (52) Setiawan, D.; Kazaryan, A.; Martoprawiro, M.; Filatov, M. *Phys. Chem. Chem. Phys.* **2010**, *12*, 11238–11244.
- (53) Vámosi, G.; Gohlke, C.; Clegg, R. M. *Biophys. J.* **1996**, *71*, 972–994.
- (54) Kuhn, H. *Angew. Chem.* **1959**, *71*, 93–101.
- (55) Çelebi, N.; Arık, M.; Onganer, Y. *J. Lumin.* **2007**, *126*, 103–108.
- (56) Arık, M.; Onganer, Y. *Chem. Phys. Lett.* **2003**, *375*, 126–133.
- (57) Kubin, R.; Fletcher, A. J. *Lumin.* **1983**, *27*, 455–462.
- (58) Glazer, A. N.; Mathies, R. A. *Curr. Op. Biotech.* **1997**, *8*, 94–102.
- (59) Eastman Laboratory Chemicals Catalog No. 55; Fisher Scientific, 1993–1994.
- (60) Birge, R. R. *Kodak Laser Dyes*; Kodak publication No. JJ-169; Kodak: Rochester, NY, 1987.
- (61) Reija, B.; Al-Soufi, W.; Novo, M.; Tato, J. J. *Phys. Chem. B* **2005**, *109*, 1364–1370.
- (62) Ribou, A.; Vigo, J.; Salmon, J. J. *Photochem. Photobiol. A* **2002**, *151*, 49–55.
- (63) Clark, J.; Miller, P.; Rumbles, G. *J. Phys. Chem. A* **1998**, *102*, 4428–4437.
- (64) Deshpande, A.; Kumar, U. *J. Lumin.* **2008**, *128*, 1121–1131.